Twisted graphene-assisted photocarrier transfer from HgSe colloidal quantum dots into silicon with enhanced collection and transport efficiency

Tang, Xin; Wu, Guang Fu; Lai, King Wai Chiu

Published in:
Applied Physics Letters

Published: 12/06/2017

Document Version:
Final Published version, also known as Publisher's PDF, Publisher's Final version or Version of Record

Published version (DOI):
10.1063/1.4986188

Publication details:
Tang, X., Wu, G. F., & Lai, K. W. C. (2017). Twisted graphene-assisted photocarrier transfer from HgSe colloidal quantum dots into silicon with enhanced collection and transport efficiency. *Applied Physics Letters*, *110*(24), 1-5. Article 241104. https://doi.org/10.1063/1.4986188

Applied Physics Letters

Twisted graphene-assisted photocarrier transfer from HgSe colloidal quantum dots into silicon with enhanced collection and transport efficiency

Cite as: Appl. Phys. Lett. **110**, 241104 (2017); https://doi.org/10.1063/1.4986188
Submitted: 09 March 2017 • Accepted: 01 June 2017 • Published Online: 14 June 2017

Xin Tang, Guang Fu Wu and King Wai Chiu Lai

Twisted graphene-assisted photocarrier transfer from HgSe colloidal quantum dots into silicon with enhanced collection and transport efficiency

Xin Tang, Guang Fu Wu, and King Wai Chiu Lai[a)]
Department of Mechanical and Biomedical Engineering, City University of Hong Kong, Hong Kong, China

(Received 9 March 2017; accepted 1 June 2017; published online 14 June 2017)

We report a strategy to realize and facilitate the photocarrier transport from mercury selenium colloidal quantum dots (HgSe CQDs) into silicon with the assistance of twisted graphene. A nanocomposite material consisting of HgSe CQDs and twisted graphene has been synthesized. By bringing the nanocomposites into contact with silicon, a HgSe CQD-twisted graphene nanocomposite/silicon junction was fabricated and demonstrated photoresponses in the long-wave infrared range. In the nanocomposites, the surface of twisted graphene was decorated with HgSe CQDs. Benefiting from the twisted structure in the nanocomposites, the active sensing area and light-matter interaction length are greatly increased. Driven by the interfacial built-in potential, photocarriers directly transfer from HgSe CQDs into the twist graphene, which serves as a fast carrier transport pathway to silicon, leading to high photocarrier collection efficiency. Compared with vertically stacked HgSe CQD film/flat graphene, the application of HgSe CQD-twisted graphene nanocomposites avoids photocarriers transporting via the hopping mechanism and over 2700% enhancement ratio of spectral responsivity was achieved, reaching 31.5 mA/W@9 μm. The interfacial energy band diagram was deduced for a better understanding of the photocarrier transfer process occurring at the interface between HgSe colloidal quantum dots, twist graphene, and silicon. *Published by AIP Publishing*. [http://dx.doi.org/10.1063/1.4986188]

The interfacial charge transfer between silicon and colloidal quantum dots (CQDs) has been extensively investigated to extend the detection limit of silicon (1.1 μm) and to develop functional optoelectronic devices.[1–4] However, the energy band mismatch and the highly defective interface between CQDs and silicon have prevented efficient photocarrier transport from CQDs to silicon, until a recent study reported that by passivating the interface with halide and organohalide compounds,[1] a favorable band alignment and interfacial charge transport were realized between PbS CQDs and silicon, extending the spectral operating range to 1.3 μm (determined by the absorption of PbS CQDs). More recently, Si:CQD photovoltage field effect transistors were demonstrated with high gain ($>10^4$), even in the infrared region with wavelengths of >1.5 μm.[5]

The large surface area (a few atomic layers[6]) and excellent carrier mobility [up to 40 000 cm^2 $V^{-1}s^{-1}$ (Ref. 7)] of graphene make it an ideal material as an interfacial layer to promote the charge transport process. The interfacial charge transfer between graphene/bulk semiconductors (Si[8,9] and Ge[10]) and graphene/CQDs has been extensively investigated for potential applications from energy harvesting to catalysts and sensors.[11,12] Numerous studies have been conducted to incorporate semiconductor CQDs (eg, PbS,[13] TiO_2,[14] CdS,[15] CdSe,[16] CdTe,[17] NiO,[18] and so on) with graphene to develop high-performance solar cells and near-infrared photodetectors. Compared with pure CQDs, 12%∼20% enhancement of photon-to-current efficiency (PCE) of CQD-graphene nanocomposite based solar cells with improved carrier mobility was demonstrated.[19–21] PbS CQD-graphene based near infrared photodetectors with an ultra-high responsivity of ∼10^7 A/W were fabricated.[22] However, for infrared with a longer wavelength, such CQD-graphene nanocomposites have rarely been reported.

In this letter, we report the synthesis of HgSe CQD-twisted graphene nanocomposites. HgSe CQDs present intraband absorption up to long-wave infrared (LWIR) with a center wavelength of 9 μm. The twisted graphene acts not only as a charge transport promotor but also as an interfacial charge transfer layer to facilitate efficient photocarrier transport from HgSe CQDs to silicon. In the nanocomposites, HgSe CQDs were on the surface of twisted graphene and the photocarriers excited in HgSe CQDs directly transfer into the twisted graphene, leading to higher collection efficiency. Benefiting from the twisted structure, graphene greatly increases the active sensing area and provides a fast transport pathway for excited photocarriers, leading to improved photocurrent generation.

HgSe CQDs with absorption up to LWIR were synthesized following a well-established protocol.[23] The synthesis was based on the reaction of mercury oleate and selenium dissolved in trioctylphosphine (TOPSe). The HgSe CQDs used in this study are approximately spherical with an average diameter of ∼14 nm, as shown by the transmission electron microscopy (TEM) image in Fig. 1(a). The infrared absorbance measurement revealed that the HgSe CQDs presented optical features of narrow intraband transition[23] in the LWIR range with a center wavelength of 9 μm [Fig. 1(b)].

The twisted graphene flakes were synthesized by reducing graphene oxide prepared by Hummers method.[24] In Fig. 1(c), the scanning electron microscopy (SEM) image shows that the lateral size of the twisted graphene flakes was ∼40 μm and micro-/nano-scale wrinkles were naturally formed during the synthesis.[25] The atomic force microscopy (AFM) height image

[a)]Author to whom correspondence should be addressed: kinglai@cityu.edu.hk

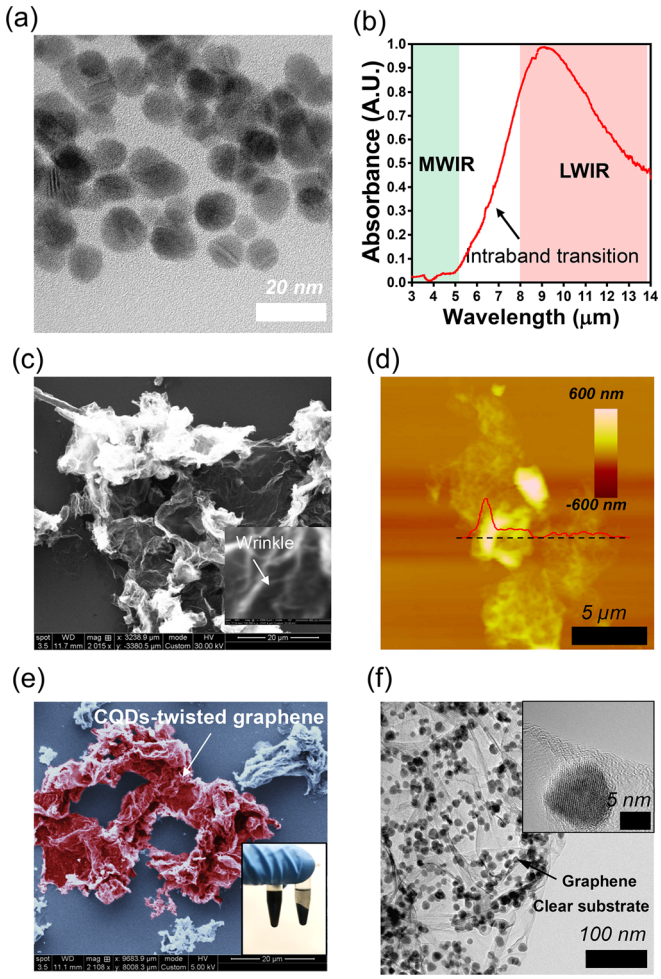

FIG. 1. (a) TEM image of the morphology of HgSe colloidal quantum dots. (b) IR absorbance of HgSe colloidal quantum dots. (c) SEM image of twisted graphene. The inset shows the high magnification SEM image of the nano-wrinkles of twisted graphene. (d) AFM height image of twisted graphene. (e) False color image of the HgSe colloidal quantum dot-twisted graphene composite. The inset shows the optical image of the CQD solution and the CQD/twisted graphene mixture. (f) TEM image of twisted graphene decorated with HgSe colloidal quantum dots. The inset shows the high-resolution TEM image.

shows that the height of twisted graphene can be a few hundreds of nanometers [Fig. 1(d)]. Therefore, the actual surface area of twisted graphene was much larger than its projected area, as a result of self-folding, wrinkles, and twists. The larger surface area and the twisted structure may facilitate the attachment of HgSe CQDs. The major advantage of twisted graphene over flat graphene is the increased light-matter interaction length. The normally incident light only passes through flat graphene one time. However, the incident light can pass through twisted graphene multiple times in different regions. The absorption efficiency can be greatly enhanced.

The HgSe CQDs were added on the twisted graphene by simply mixing the graphene samples with the HgSe CQD solution. Initially, the HgSe CQDs were capped with dodecanethiol (DDT). After the ligand exchange process, the long-chain DDT is changed to ethanedithiol (EDT). Previous studies have demonstrated that the short-chain ligands can facilitate efficient charge transfer from CQDs to graphene.[13,22,26] The details of the synthesis process are given in the supplementary material (Fig. S1). The false-color SEM image highlights one twisted graphene conjugated with HgSe CQDs [Fig. 1(e)]. The main structural features (twisted structure) were preserved after the mixing process. As shown in the inset of Fig. 1(e), the left tube contained the HgSe CQD solution. After adding the twisted graphene to the HgSe CQD solution, precipitation was observed (right tube). The upper clear solution was solvent, and the lower dark parts were the HgSe CQD-twisted graphene nanocomposites. The distribution of HgSe CQDs on the twisted graphene was revealed in the TEM image [Fig. 1(f)]. The HgSe CQDs were observed on the surface of graphene. We speculated that the interaction forces between HgSe CQDs and twisted graphene were mainly van der Waals force[27,28] and electrostatic force.[29]

To gain a comprehensive understanding of the function of twisted graphene in the photocarrier transfer process from HgSe CQDs to silicon, three types of junctions were constructed and studied: HgSe CQD film/Si junction (HSJ), HgSe CQD film-flat graphene/Si junction (FFG/Si junction), and HgSe CQD-twisted graphene nanocomposite/Si junction (TG/Si junction). The cross-view of the three junction structures is illustrated in Figs. 2(a)–2(c). The HSJ was fabricated by directly transferring the patterned HgSe film onto the silicon chip with electrodes by the poly(methyl methacrylate) (PMMA)-assisted transfer process [Fig. 1(d)]. The same PMMA transfer process could also be used to fabricate lateral metal/CQD film/metal devices, as reported in our previous studies.[30,31] The FFG/Si junction was fabricated by two steps of the transfer process: the flat graphene was transferred to the electrodes followed by the transfer of the HgSe CQD film. The false color SEM image shows the top view of the fabricated FFG/Si junction [Fig. 2(e)]. The three-layer structure is clearly shown in the inset of Fig. 2(e). A flat graphene layer was inserted between the HgSe CQD film and silicon. The TG/Si junction was fabricated by drop-casting the HgSe CQD-twisted graphene solution onto the electrodes. This drop-casting process was repeated 10 times for all TG/Si junctions to optimize the photoresponse by increasing the density of nanocomposites. The inter-finger gap of the electrodes is $\sim 30\,\mu$m, allowing the HgSe CQD-twisted graphene flakes to bridge the electrodes and silicon at the same time as shown in Fig. 2(f). More details of the fabrication process are shown in the supplementary materials.

In order to study the photocarrier transport behaviors in the three fabricated junctions, the photoresponses were measured. The blackbody system (Newport Oriel 67032) with narrowband optical filters was used as the light source. The photocurrent was measured using a semiconductor analyzer (Keysight B1500A). As shown in the inset of Fig. 2(d), the constructed HSJ showed a rectifying IV curve, but no photocurrent was measured upon LWIR illumination, indicating an interfacial energetic barrier which may block the photocarrier transport from HgSe CQDs into silicon. For the other two junctions, extraction of photocarriers from HgSe CQDs into silicon via graphene was experimentally demonstrated. To confirm that the measured photoresponse is resulted from the HgSe CQDs, the flat graphene/silicon junction and the twisted graphene/silicon junction were investigated and both junctions showed no photoresponse in the LWIR range,

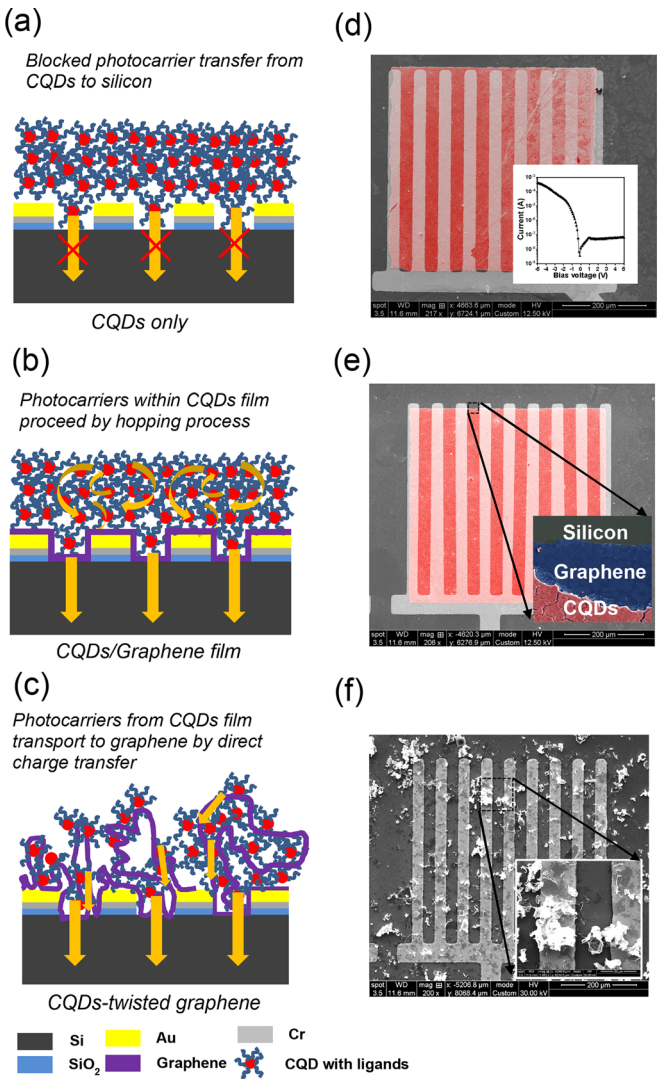

FIG. 2. (a) The cross-view of HSJ. (b) The cross-view of the FFG/Si junction. (c) The cross-view of the TG/Si junction. (d) False color SEM image of HSJ. The red region denotes the HgSe CQD film. The inset shows the rectifying IV curve of the junction. (e) False color SEM image of the FFG/Si junction. The red region denotes the HgSe CQD film. The inset shows the zoom view of the three-layer structure of HgSe CQD/graphene/silicon. (f) SEM image of the TG/Si junction. The inset shows the zoom view of the HgSe CQD-twisted graphene nanocomposite.

limited by the weak optical absorption of graphene (2.3% per layer[6]) and Pauli blocking of doped graphene.[32]

Although photocurrent was extracted from the FFG/Si junction, the magnitude of responsivity of the FFG/Si junction is much lower than that of the TG/Si junction. It can be due to distinct photocarrier transfer efficiency between the two junctions. For the FFG/Si junction, the responsivity gradually increases with the thickness of the HgSe CQD film until saturation (thickness > 170 nm) and the saturated responsivity at 9 μm was ~0.356 mA/W [Fig. 3(a)]. Therefore, in our experiments, the optimal thickness of the HgSe CQD film in the FFG/Si junction was 170 nm. We speculated that the optimal thickness was determined by two competing factors: overall collection efficiency and the number of photoexcited carriers. Since the carrier diffusion length in the HgSe CQD film was limited, the collection efficiency of photocarriers excited away from the graphene should decay rapidly. Therefore, the thin HgSe CQD film may have higher overall photocarrier

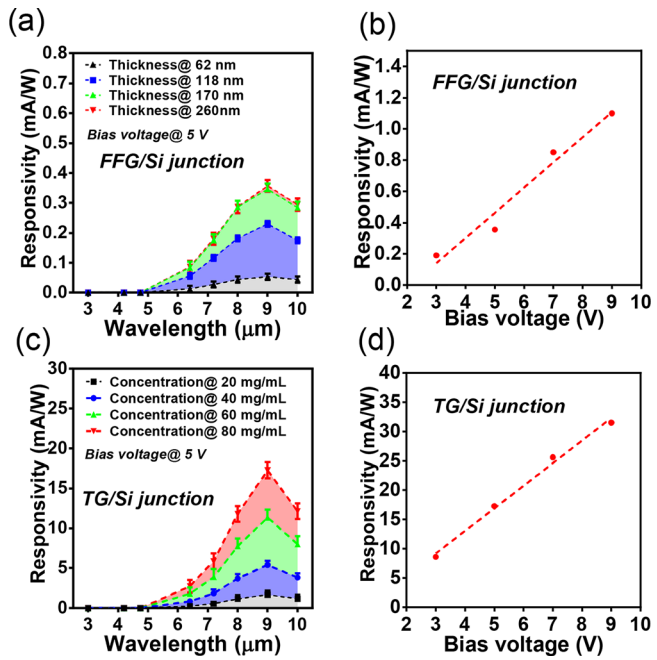

FIG. 3. (a) The spectral responsivity as a function of the thickness of HgSe CQD films (N= 8). (b) Bias voltage-dependent responsivity at a wavelength of 9.0 μm of the FFG/Si junction. (c) The spectral responsivity as a function of the concentration of HgSe CQD solution (N= 8). (d) Bias voltage-dependent responsivity at a wavelength of 9.0 μm of the TG/Si junction.

collection efficiency than the thick HgSe CQD film. However, as the thickness increased, although the overall carrier collection efficiency decreased, the number of generated photocarriers increased. Consequently, the photoresponse of the FFG/Si junction gradually increased with the thickness of HgSe CQD films, until the increased photocarriers excited from the upper part of the HgSe CQDs cannot be collected by the bottom graphene, which was consistent with the experimental results. More details of the photocarrier transport can be found in the supporting information. By increasing the bias voltage, the responsivity of the FFG/Si junction at a bias of 9 V increased to 1.17 mA/W [Fig. 3(b)]. Figure 3(c) shows the spectral responsivity of the TG/Si junction as a function of the concentration of HgSe CQD solution used to prepare the nanocomposites. The increased concentration of HgSe CQDs caused a higher density of HgSe CQDs on twisted graphene and resulted in a higher photocarrier generation rate. When the concentration of HgSe CQDs (used to prepare the HgSe CQD-twisted graphene composite) was increased from 20 mg/ml to 80 mg/ml, the responsivity increased and reached 17.28 mA/W at 9 μm. By increasing the bias voltage from 5 V to 9 V, the responsivity increased almost 2 times, reaching 31.5 mA/W [Fig. 3(d)].

Compared to the FFG/Si junction, the responsivity at 9 μm of the TG/Si junction is enhanced by around 2700%. We ascribe this large enhancement ratio to several advantages of the HgSe CQD-twisted graphene nanocomposite. The first advantage is the high photocarrier transfer efficiency from the HgSe CQDs to the twisted graphene. As shown in Figs. 1(f) and 2(c), the HgSe CQDs were on the surface of twisted graphene and the photocarrier can directly transfer into graphene without the hopping process. Therefore, all the HgSe CQDs attached on the graphene efficiently contributed photocarriers

and the active sensing area was the whole surface area of the twisted graphene. More importantly, the twisted graphene provided a fast carrier transport path for the photocarriers transferred from HgSe CQDs. In our experiments, the carrier mobility of twisted graphene was in the range of 12.7–43.1 $cm^2\ V^{-1}s^{-1}$, which was much larger than that of HgSe CQDs (0.85–5 $\times 10^{-4}$ $cm^2\ V^{-1}s^{-1}$). More details can be found in the supporting information. In contrast, photocarriers within the HgSe CQD-flat graphene proceeded via hopping between adjacent HgSe CQDs.[33] To arrive at the flat graphene, photocarriers must undergo multiple hopping processes without recombination and trapped-state termination (low carrier transport efficiency). Therefore, only a thin layer of HgSe CQDs near the flat graphene was the active sensing area. HgSe CQDs far from graphene (>170 nm) barely contributed to photocarriers. Second, compared to flat graphene with the same sensing area on the chip, the twisted graphene had a much larger surface area benefiting from the wrinkles and self-folding. Therefore, the total active sensing area of the TG/Si junction is much larger than that of the FFG/Si junction. Third, during the synthesis of twisted graphene, the reduction process may introduce defects and functionalization groups on the surface of graphene,[34] which may create more bonding sites and facilitate the charge transfer from the HgSe CQDs and the twisted graphene.

To further understand the photocarrier transfer process, the interfacial energy band diagram was deduced. The synthesized HgSe CQDs are naturally n-doped. The doping level and the work function of HgSe CQDs can be influenced by the magnitude of surface dipoles, which originated from the ligand materials.[35] A previous study has demonstrated tunable work functions of HgSe CQDs (not composited with other materials) from ~5.0 to ~5.7 eV by controlling the ligand materials.[35] To experimentally determine the relative position of Fermi levels between EDT-capped HgSe CQDs and graphene in the nanocomposites, the gate dependent transfer curve of graphene before and after adding the HgSe CQDs was measured.[13,22,26] An obvious shift of Dirac voltage from 22.5 V to 8 V (n doping effect) was observed as shown in Fig. 4(a). The results indicated electron transfer from HgSe colloidal quantum dots to graphene due to the difference in the work function of the two materials.[36,37] Therefore, we assume that the work function of HgSe CQDs used in this study should be smaller than that of graphene. The work function of graphene $W_{graphene}$ can be calculated by[38]

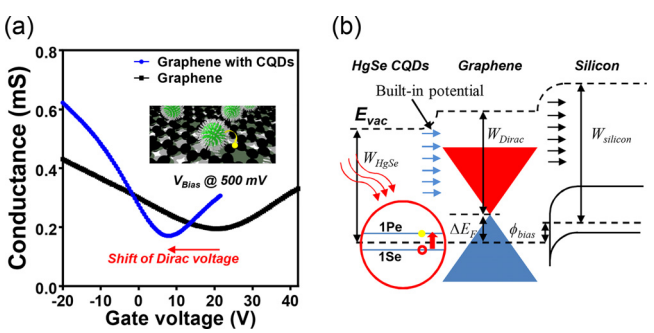

FIG. 4. (a) Gate-dependent transfer curve of graphene with/without HgSe quantum dots. (b) Energy band diagram of the CQD-graphene/silicon heterojunction.

$$W_{graphene} = W_{Dirac} + \Delta E_F = W_{Dirac} + \mathrm{sgn}(n_0)\hbar v_F \sqrt{\pi |n_0|}, \quad (1)$$

where W_{Dirac} is the work function of graphene at the Dirac point [~4.8 eV (Ref. 39)], ΔE_F is the Fermi level shift in graphene relative to the Dirac point, $\hbar$ is the reduced Planck constant, v_F is the Fermi velocity [$\sim 1.1 \times 10^6$ m/s (Ref. 38)], and the carrier density n_0 is defined to be positive for holes and negative for electrons. The work function of graphene before and after the addition of HgSe CQDs can be calculated to be 5.05 and 4.95 eV, respectively. When the equilibrium state is reached, a depletion region and band bending should be formed in HgSe CQDs as shown in Fig. 4(b). The interfacial built-in potential is denoted by the blue arrow. The interfacial energy band diagram of graphene and p-type silicon was already well-established.[40,41] The bias voltage applied between graphene and silicon leads to an offset energy barrier between the Fermi energy of graphene and silicon. When the photon energy of LWIR was absorbed by the HgSe CQDs, the electron in the $1S_e$ state was excited into $1P_e$, generating photocarriers. With the assistance of twisted graphene, interfacial photocarrier transport between the HgSe CQDs and silicon was realized, resulting in measurable photocurrents.

In summary, the HgSe CQD-twisted graphene nanocomposite was synthesized by a simple mixing process. The HgSe CQD-twisted graphene nanocomposite/silicon junction was fabricated, and we have demonstrated that the twisted graphene can assist photocarrier transfer from the HgSe CQDs to silicon. In the HgSe CQD-twisted graphene nanocomposite, the twisted graphene acts as an excellent interfacial charge transport layer and scaffold to provide a large active sensing area. Benefiting from the twisted structure of graphene, over 2700% enhancement ratio of spectral responsivity was achieved, reaching 31.5 mA/W. The interfacial energy band diagram was deduced for a better understanding of the photocarrier transfer process. We believe that these findings contribute to a deeper understanding of the interfacial charge transport between graphene and other active components and the use of twisted graphene-CQD nanocomposites to build up high-performance solar cells and photodetectors.

See supplementary material for the synthesis of the HgSe CQD-twisted graphene nanocomposite, fabrication process for the HSJ, FFG/Si junction, and TG/Si junction, photocarrier transport, gate-dependent transfer curve measurement configuration, and calculation of carrier mobility.

This research was partially supported by the GRF grant from the Research Grant Council of the Hong Kong Special Administrative Region Government (CityU139313 and CityU11205514).

[1]S. Masala, V. Adinolfi, J. Sun, S. Del Gobbo, O. Voznyy, I. J. Kramer, I. G. Hill, and E. H. Sargent, Adv. Mater. **27**, 7445 (2015).
[2]T. Song, F. Zhang, X. Lei, Y. Xu, S. Lee, and B. Sun, Nanoscale **4**, 1336 (2012).
[3]C.-Y. Huang, D.-Y. Wang, C.-H. Wang, Y.-T. Wang, Y.-T. Jiang, Y.-J. Yang, C.-C. Chen, and Y.-F. Chen, J. Phys. D: Appl. Phys. **44**, 85103 (2011).
[4]H.-C. Chen, C.-C. Lin, H.-W. Han, Y.-L. Tsai, C.-H. Chang, H.-W. Wang, M.-A. Tsai, H.-C. Kuo, and P. Yu, Opt. Express **19**, A1141 (2011).

[5]V. Adinolfi and E. H. Sargent, Nature **542**, 324 (2017).
[6]a. K. Geim and K. S. Novoselov, Nat. Mater. **6**, 183 (2007).
[7]H. Lv, H. Wu, J. Liu, J. Yu, J. Niu, J. Li, Q. Xu, X. Wu, and H. Qian, Appl. Phys. Lett. **103**, 193102 (2013).
[8]X. Liu, X. W. Zhang, Z. G. Yin, J. H. Meng, H. L. Gao, L. Q. Zhang, Y. J. Zhao, and H. L. Wang, Appl. Phys. Lett. **105**, 183901 (2014).
[9]X. Tang, H. Zhang, X. Tang, and K. W. C. Lai, Mater. Res. Express **3**, 76203 (2016).
[10]L.-H. Zeng, M.-Z. Wang, H. Hu, B. Nie, Y.-Q. Yu, C.-Y. Wu, L. Wang, J.-G. Hu, C. Xie, and F.-X. Liang, ACS Appl. Mater. Interfaces **5**, 9362 (2013).
[11]W. Yang, K. R. Ratinac, S. P. Ringer, P. Thordarson, J. J. Gooding, and F. Braet, Angew. Chem. Int. Ed. **49**, 2114 (2010).
[12]X. Huang, X. Qi, F. Boey, and H. Zhang, Chem. Soc. Rev. **41**, 666 (2012).
[13]D. Zhang, L. Gan, Y. Cao, Q. Wang, L. Qi, and X. Guo, Adv. Mater. **24**, 2715 (2012).
[14]K. K. Manga, S. Wang, M. Jaiswal, Q. Bao, and K. P. Loh, Adv. Mater. **22**, 5265 (2010).
[15]A. Cao, Z. Liu, S. Chu, M. Wu, Z. Ye, Z. Cai, Y. Chang, S. Wang, Q. Gong, and Y. Liu, Adv. Mater. **22**, 103 (2010).
[16]Y. Lin, K. Zhang, W. Chen, Y. Liu, Z. Geng, J. Zeng, N. Pan, L. Yan, X. Wang, and J. G. Hou, ACS Nano **4**, 3033 (2010).
[17]Z. Lu, C. X. Guo, H. Bin Yang, Y. Qiao, J. Guo, and C. M. Li, J. Colloid Interface Sci. **353**, 588 (2011).
[18]H. Yang, G. H. Guai, C. Guo, Q. Song, S. P. Jiang, Y. Wang, W. Zhang, and C. M. Li, J. Phys. Chem. C **115**, 12209 (2011).
[19]B.-S. Kim, D. C. J. Neo, B. Hou, J. B. Park, Y. Cho, N. Zhang, J. Hong, S. Pak, S. Lee, and J. I. Sohn, ACS Appl. Mater. Interfaces **8**, 13902–13908 (2016).
[20]A. Mnoyan, K. Kim, J. Y. Kim, and D. Y. Jeon, Sol. Energy Mater. Sol. Cells **144**, 181 (2016).
[21]S. Giménez, I. Mora-Seró, L. Macor, N. Guijarro, T. Lana-Villarreal, R. Gómez, L. J. Diguna, Q. Shen, T. Toyoda, and J. Bisquert, Nanotechnology **20**, 295204 (2009).
[22]G. Konstantatos, M. Badioli, L. Gaudreau, J. Osmond, M. Bernechea, F. P. G. de Arquer, F. Gatti, and F. H. L. Koppens, Nat. Nanotechnol. **7**, 363 (2012).
[23]E. Lhuillier, M. Scarafagio, P. Hease, B. Nadal, H. Aubin, X. Z. Xu, N. Lequeux, G. Patriarche, S. Ithurria, and B. Dubertret, Nano Lett. **16**, 1282 (2016).
[24]W. S. Hummers, Jr. and R. E. Offeman, J. Am. Chem. Soc. **80**, 1339 (1958).
[25]Y. Zhu, W. Cai, R. D. Piner, A. Velamakanni, and R. S. Ruoff, Appl. Phys. Lett. **95**, 103104 (2009).
[26]Z. Sun, Z. Liu, J. Li, G. Tai, S. Lau, and F. Yan, Adv. Mater. **24**, 5878 (2012).
[27]G. A. Rance, D. H. Marsh, S. J. Bourne, T. J. Reade, and A. N. Khlobystov, ACS Nano **4**, 4920 (2010).
[28]S. Mukherjee, R. Maiti, A. K. Katiyar, S. Das, and S. K. Ray, Sci. Rep. **6**, 29016 (2016).
[29]L. Li, K. Liu, G. Yang, C. Wang, J. Zhang, and J. Zhu, Adv. Funct. Mater. **21**, 869 (2011).
[30]X. Tang, X. Tang, and K. W. C. Lai, ACS Photonics **3**, 2396 (2016).
[31]X. Tang, G. fu Wu, and K. W. C. Lai, J. Mater. Chem. C **5**, 362 (2017).
[32]Q. Bao, H. Zhang, Y. Wang, Z. Ni, Y. Yan, Z. X. Shen, K. P. Loh, and D. Y. Tang, Adv. Funct. Mater. **19**, 3077 (2009).
[33]I. Carbone, S. A. Carter, and G. T. Zimanyi, J. Appl. Phys. **114**, 193709 (2013).
[34]O. C. Compton and S. T. Nguyen, Small **6**, 711 (2010).
[35]A. Robin, C. Livache, S. Ithurria, E. Lacaze, B. Dubertret, and E. Lhuillier, ACS Appl. Mater. Interfaces **8**, 27122 (2016).
[36]Y. Shi, K. K. Kim, A. Reina, M. Hofmann, L.-J. Li, and J. Kong, ACS Nano **4**, 2689 (2010).
[37]H. Liu, Y. Liu, and D. Zhu, J. Mater. Chem. **21**, 3335 (2011).
[38]Y. An, A. Behnam, E. Pop, and A. Ural, Appl. Phys. Lett. **102**, 13110 (2013).
[39]S. Pang, H. N. Tsao, X. Feng, and K. Müllen, Adv. Mater. **21**, 3488 (2009).
[40]C.-C. Chen, M. Aykol, C.-C. Chang, A. F. J. Levi, and S. B. Cronin, Nano Lett. **11**, 1863 (2011).
[41]X. An, F. Liu, Y. J. Jung, and S. Kar, Nano Lett. **13**, 909 (2013).